Simultaneous Viscous-Inviscid Interaction Calculation Procedure for Transonic Turbulent Flows

D. Lee* and R. H. Pletcher†
Iowa State University, Ames, Iowa

A new simultaneous viscous-inviscid interaction scheme has been developed for the analysis of steady turbulent transonic separated flows. The viscous and inviscid solutions are coupled through the displacement concept using a transpiration velocity. The local solutions of the full potential and boundary-layer equations are treated simultaneously using the finite-difference method. The displacement thickness is treated as an unknown and is obtained as a part of the solution through a global iteration procedure of the space-marching scheme. The Cebeci-Smith and Johnson-King models are used in the turbulent flow calculations. The computational examples indicate that the simultaneous method is more efficient and robust than the semi-inverse method for transonic flows with a strong interaction.

Nomenclature

b = exponent, Eq. (16)
c_f = skin-friction coefficient
C = chord length of the bump
C_p = pressure coefficient
d_m = maximum boattail diameter
F,G = nondimensional u and H, Eq. (2)
g = function used in Eq. (1)
H = total enthalpy
m = mass flux parameter, $\rho_e u_e r_0 \delta^*$
M = Mach number
Pr = Prandtl number
r = radius
Re = Reynolds number based on the freestream and unit length (1 m)
s,n = curvilinear coordinates
t = depth of a trough, Eq. (17)
u,v = velocity components in (s,n) coordinates
x,y = Cartesian coordinates
β = pressure gradient parameter, Eq. (4)
γ = ratio of specific heat
δ^* = displacement thickness
ε = convergence criterion
μ = viscosity
ξ,η = transformed coordinates
ρ = density
ϕ = velocity potential
ψ = stream function
ω = relaxation factor

Subscripts and Superscripts

e = edge of the boundary layer
i,j = indices of grid point
I = inviscid
t = turbulent
V = viscous
∞ = freestream conditions
n = iteration index

Received May 22, 1987; presented as Paper 87-1155-CP at the AIAA 8th Computational Fluid Dynamics Conference, Honolulu, HI, June 9–11, 1987; revision received March 18, 1988.

*Research Assistant, Department of Mechanical Engineering and Computational Fluid Dynamics Center. Currently Senior Scientist, Avco Research Laboratory, Inc., Everett, MA. Member AIAA.

†Professor, Department of Mechanical Engineering and Computational Fluid Dynamics Center. Member AIAA.

I. Introduction

ACCURATE analysis of transonic flows has been in demand over the last few decades as the occurrence of transonic flow in aerodynamic applications has grown. The structure of transonic flows often becomes complex due to the interaction of a boundary layer with a shock wave, which often causes separation. The computational strategies for transonic flows can be divided into global and zonal approaches. In the first approach, the flowfield is computed with a single set of equations, such as the Reynolds-averaged Navier-Stokes equations, valid everywhere without special assumptions concerning the type or nature of interaction. Generally, the Navier-Stokes solutions provide reasonably good predictions for flows with strong interaction between a shock wave and a boundary layer. However, the Navier-Stokes solution often requires a large computational effort despite the progress made in recent years. In the zonal approach, the flow is divided into subregions with distinct flow characteristics. Each subregion is then described by an appropriately reduced set of governing equations. It is often possible to solve these two sets of equations interactively in a consistent manner using the viscous-inviscid interaction approach. Predictions based on this approach generally compare well with the solutions of the Navier-Stokes equations.

An objective of the study is to develop a robust and efficient viscous-inviscid interaction scheme that can be used to predict transonic turbulent flows with strong interaction between a shock wave and a boundary layer. Among the several proposed interaction schemes (see Ref. 1 for a review), the semi-inverse method, developed by Le Balleur[2] and Carter,[3] has gained popularity. In this method, the boundary-layer equations are solved inversely with the prescribed displacement thickness and the inviscid flow is solved in the direct mode. A coupling algorithm is then devised to update the displacement thickness in a manner that will reduce the difference between the two solutions at the next iteration. However, the coupling algorithms used in the semi-inverse methods to date have been rather arbitrary and lack a rigorous theoretical background. Also, according to the stability

analysis done by Wigton and Holt,[4] the semi-inverse method of Carter[3] becomes unstable for large separated flow regions in a supersonic stream.

For strongly interacting flows, a localized implicit treatment of coupling between the viscous and inviscid regions seems to be preferable. This approach, which seeks a simultaneous solution of the viscous and inviscid flow regions, is classified broadly as a simultaneous interaction method. Most of the simultaneous methods[5-8] developed to date have used integral methods for either the viscous or inviscid flow equations. A fully finite-difference simultaneous method was first introduced by Edwards and Carter[9] for incompressible separated flow calculations. No solution schemes of this kind have been noted yet for transonic flows. In the present study, a simultaneous interaction method is developed for the finite-difference representation of the equations for viscous and inviscid regions for transonic flow. The effectiveness of the new simultaneous method is compared with the semi-inverse method for both incompressible and transonic flows over several different body configurations.

The accuracy and reliability of turbulent flow predictions are also very much constrained by the accuracy and generality of the turbulence model. Surprisingly, complex models[10] do not provide significant improvement over algebraic models for transonic flows with large separation. In the present study, a new turbulence model proposed by Johnson and King[11] is evaluated in comparison with the algebraic Cebeci-Smith model.[12]

II. Analysis

Viscous Flow

The boundary-layer equations are used to describe the flow in the viscous region. The formulation of the mean boundary-layer equations for the steady, axisymmetric, compressible, turbulent flow written in curvilinear coordinates (s,n) is given in Ref. 12. When the boundary-layer equations are recast with similarity-type independent variables defined as

$$\xi = \int_0^s \rho_e \mu_e u_e r_0^2 \, ds, \qquad \eta = \frac{u_e}{g} \int_0^n \rho r \, dn \tag{1}$$

the stagnation point singularity can be removed, and more gradual growth of the boundary layer in the computational coordinates can be provided by the proper choice of g. With the definitions of the stream function and new dependent variables,

$$\frac{\partial \psi}{\partial s} = -\rho v r, \qquad F = \frac{u}{u_e}, \qquad G = \frac{H}{H_e} \tag{2}$$

the boundary-layer equations can be expressed as

$$gF = \frac{\partial \psi}{\partial \eta} \tag{3a}$$

$$g^2 F \frac{\partial F}{\partial \xi} - g \frac{\partial \psi}{\partial \xi} \frac{\partial F}{\partial \eta} = g^2 \beta (G - F^2) + \frac{\partial}{\partial \eta}\left[C_\ell \left(1 + \frac{\mu_t}{\mu}\right) \frac{\partial F}{\partial \eta} \right] \tag{3b}$$

$$g^2 F \frac{\partial G}{\partial \xi} - g \frac{\partial \psi}{\partial \xi} \frac{\partial G}{\partial \eta} = \frac{\partial}{\partial \eta}\left[\frac{C_\ell}{Pr} \left(1 + \frac{\mu_t Pr}{\mu Pr_t}\right) \frac{\partial G}{\partial \eta} \right] + C_E \frac{\partial}{\partial \eta}\left\{ C_\ell \left[\left(1 - \frac{1}{Pr}\right) + \left(1 - \frac{1}{Pr_t}\right) \frac{\mu_t}{\mu} \right] F \frac{\partial F}{\partial \eta} \right\} \tag{3c}$$

where

$$\beta = \frac{1}{M_e} \frac{dM_e}{d\xi}, \qquad C_\ell = \frac{\rho \mu}{\rho_e \mu_e} \left(\frac{r}{r_0}\right)^2, \qquad C_E = \frac{(\gamma - 1) M_e^2}{1 + 0.5(\gamma - 1) M_e^2} \tag{4}$$

The boundary conditions are given as

$$F = \psi = 0, \qquad G = G_w \qquad \text{at } \eta = 0 \tag{5a}$$

$$F = G = 1.0 \qquad \text{at } \eta \to \infty \tag{5b}$$

The classical separation singularity can be avoided by using the inverse formulation. The inverse method used in the present study is based on the procedure of Ref. 13. From the definition of the displacement thickness, the stream function at the edge of the boundary layer can be expressed as

$$\psi_e = g \int_0^{n_e} \left(\frac{\rho_e}{\rho}\right) d\eta - m \tag{6}$$

where the mass flux parameter $m = \rho_e u_e r_0 \delta^*$.

The turbulent shear stress and heat flux terms are related to the mean flow using a turbulent viscosity μ_t and turbulent Prandtl number Pr_t. The algebraic two-layer Cebeci-Smith[12] and Johnson-King models[11] are used to describe the turbulent viscosity. The form of the Cebeci-Smith model is given in Ref. 12. Transonic turbulent flow is usually characterized by strong upstream effects. The Cebeci-Smith model is known to predict rather poorly in such flows mainly due to the assumption of local equilibrium between the mean flow motion and the local turbulence. Johnson and King[11] suggested a new turbulence model for flows in strong adverse pressure gradients. In this model, $-\overline{u'v'}_m$ determined from the solution of an ordinary differential equation that is derived from the turbulent kinetic-energy equation serves as a velocity scale for the turbulent viscosity. The details of this model are given in Refs. 11, 14, and 15. It should be noted that for turbulent flows, transition from laminar to turbulent flow is assumed to occur at a fixed point near the leading edge without the use of a particular formula for the transition point. Also, a constant value of turbulent Prandtl number ($Pr_t = 0.95$) is used.

The boundary-layer equations given above are solved using a fully implicit finite-difference scheme, which is first-order-accurate in the streamwise direction and second-order-accurate in the transverse direction. The continuity and momentum equations are solved in a coupled manner using Newton linearization. The energy equation and the transport equation for the turbulent model are solved in an uncoupled manner. It was initially found that most of the computing time in the simultaneous interaction method was consumed by the local iterations of the Newton linearization. In order to reduce the computing time needed in the linearization procedure, a pseudo-time-dependent approach was developed. In this approach, the initial value needed to start the linearization process is taken from solutions of the previous interaction sweep, not from the solutions at the upstream station (lagging). The global interaction procedure is started by using conventional space lagging for the Newton linearization and then switched to the pseudo-time approach if the convergence level for the interaction process, measured based on the relative change in m, is less than 5%. This remedy proved to be so efficient that the total computing time was reduced by a factor of 5 in typical transonic flow cases.

Equations (3) are parabolic and can be solved in a forward-marching manner in the streamwise direction when $F > 0$. In the reversed flow region, the solution can be advanced in the positive coordinate direction only iteratively using a windward-differencing representation for convective terms that honors the appropriate marching direction. A much simpler alternative to the windward differencing is to neglect the streamwise convective term when $F < 0$ according to the FLARE approximation, first suggested by Reyhner and Flügge-Lotz.[16] In the present calculations, the FLARE approximation is generally used, and its effectiveness is evaluated by comparing with the results of the windward-differencing scheme for flows with large separated regions.

Coupling of the continuity and momentum equations forms a block linear tridiagonal system with each block consisting of a 2×2 matrix. Using the block elimination procedure, the tridiagonal system is reduced to a bidiagonal recurrence form as

$$F_j^i = a_j F_{j+1}^i + b_j \beta + c_j g + d_j \tag{7a}$$

$$\psi_j^i = a'_j F_{j+1}^i + b'_j \beta + c'_j g + d'_j \tag{7b}$$

By letting $g = m$ and applying Eq. (6) and the boundary conditions, a local relationship between β and m is obtained as

$$\beta = a_v m + b_v \tag{8}$$

The values of β and m are determined so as to satisfy an additional relationship between β and m that will be derived from the inviscid analysis. When β and m are known, solutions for various F and ψ across the boundary layer can be obtained by the simple back-substitution procedure starting from the edge of the boundary using the boundary conditions and proceeding toward the wall.

Inviscid Flow

With the assumption of a steady, irrotational, isentropic flow without body forces or external heat transfer, the inviscid flow region is governed by a full potential equation. The full potential equation in conservative form can be written in an axisymmetric cylindrical coordinate system as

$$(\rho \phi_x r)_x + (\rho \phi_r r)_r = 0 \tag{9a}$$

$$\rho = \left[1 - \frac{\gamma - 1}{\gamma + 1} (\phi_x^2 + \phi_r^2) \right]^{1/(\gamma - 1)} \tag{9b}$$

where the density ρ and velocity potential ϕ are nondimensionalized by the stagnation and critical speed of sound, respectively. The velocity potentials at the inflow and upper boundaries are determined by the uniform freestream condition. The outflow boundary is also positioned such that the streamwise variation of the flow is set to be zero. Following the analysis of Lighthill,[17] the boundary condition at the lower boundary along the body surface is given by the transpiration velocity:

$$\phi_r(r = r_0) = \frac{1}{\rho_e r_0} \frac{\mathrm{d}}{\mathrm{d}s} (\rho_e u_e r_0 \delta^*) = \frac{1}{\rho_e r_0} \frac{\mathrm{d}m}{\mathrm{d}s} \tag{10}$$

Use of the transpiration-velocity condition not only eliminates the need for iterative generation of meshes but also makes it possible to derive the explicit local relationship between the pressure gradient and the displacement thickness needed for the present simultaneous interaction scheme.

Equation (9) is transformed into the computational domain using general independent variables (ξ, η) and is discretized with second-order-accurate central-difference approximations. In order to provide the upwind bias in differencing of the streamwise terms in supersonic regions, the density coefficients are replaced by the artificial retarded-density coefficients as suggested by Holst and Ballhaus.[18] A nonorthogonal, body-fitted mesh is established by using the numerical grid-generation scheme introduced by Thompson et al.[19] The mesh is constructed so that more grid points are concentrated where the gradients of flow properties are expected to be large. The resulting finite-difference form of the full potential equation is solved by a conventional, simple successive line overrelaxation (SLOR) scheme. Even though the SLOR scheme is considered relatively inefficient compared to other relaxation methods, it simplifies the local treatment of the coupling procedure. Applying the SLOR scheme results in a tridiagonal matrix equation for each $\xi = \text{constant}$ line. After elimination of upper diagonal terms in the coefficient matrix, a bidiagonal recurrence relationship at iteration level $n + 1$ is obtained as

$$\phi_{i,j}^{n+1} = B_j + D_j \phi_{i,j-1}^{n+1} \tag{11}$$

Implementation of the inner boundary condition leads to a linear relationship between the local potential and the gradients of the mass flux parameter at the ith column:

$$\phi_{i,1}^{n+1} = p_0 + p_1 \left(\frac{\mathrm{d}m}{\mathrm{d}\xi} \right)_{i-\frac{1}{2}} + p_2 \left(\frac{\mathrm{d}m}{\mathrm{d}\xi} \right)_i + p_3 \left(\frac{\mathrm{d}m}{\mathrm{d}\xi} \right)_{i+\frac{1}{2}} \tag{12}$$

If the distribution of m is known, then values of ϕ^{n+1} at the ith column can be calculated recursively using Eq. (11). The SLOR procedure then proceeds to the next $(i + 1)$ column to continue the streamwise sweep.

Viscous-Inviscid Interaction Method

A coupling procedure is needed to determine the appropriate value of m so that the solutions from the viscous and inviscid regions match. In the present work, the new simultaneous and the semi-inverse interaction methods are used. The simultaneous interaction method is described below.

By using a finite-difference approximation for $\mathrm{d}m/\mathrm{d}\xi$ in Eq. (12), $\phi_{i,1}$ can be expressed in terms of m. Among the $\mathrm{d}m/\mathrm{d}\xi$ terms in Eq. (12), $(\mathrm{d}m/\mathrm{d}\xi)_i$ has the most significant effect on the accuracy and stability of the solution because this term is directly associated with the transpiration velocity. This term is discretized by a second-order-accurate backward-differencing formula. The other two terms appearing due to the skewness of the mesh cell are approximated by second-order-accurate central-differencing formulas based on the previously known distribution of m. As a result, $\phi_{i,1}$ is expressed as a function of local m_i as

$$\phi_{i,1}^{n+1} = \lambda_1 m_i + \lambda_2 \tag{13}$$

Using a central finite-difference expression, the pressure gradient parameter β is also approximated in terms of the velocity potential as

$$\beta = R_{i+\frac{1}{2}} (\phi_{i+1,1}^n - \phi_{i,1}^n) - R_{i-\frac{1}{2}} (\phi_{i,1}^{n+1} - \phi_{i-1,1}^{n+1}) \tag{14}$$

Substituting Eq. (13) into Eq. (14) and combining all known quantities, the local relationship between β and m in the inviscid flowfield can be written in the following form:

$$\beta = a_I m + b_I \tag{15}$$

Requiring that the inviscid and viscous pressure gradients be the same, the new values of m and β can be determined from Eqs. (8) and (15). Then the solutions of the viscous and inviscid flow at the local streamwise station can be obtained recursively as described above. Since Newton linearization is used in boundary-layer equations, the viscous relationship, Eq. (8), has to be iteratively updated at each streamwise station until the local solution converges. On the other hand, the inviscid relationship, Eq. (15), does not need to be iteratively updated. However, a relaxation factor ω is applied to the converged m_i when the new value of $\phi_{i,1}$ is calculated. The convergence rate of the global iteration process is very sensitive to the choice of the relaxation factor. The optimum value was determined by trial-and-error and ranged from 0.4 to 0.75 in the present study. The above procedure is then applied to the next streamwise $(i + 1)$ station. This overall sweep procedure is iteratively repeated in order to account for elliptic effects. The skeleton flowchart for this simultaneous interaction method is shown in Fig. 1.

The semi-inverse interaction method is also employed so that the relative performance of the above new simultaneous method can be assessed. The semi-inverse method used in the

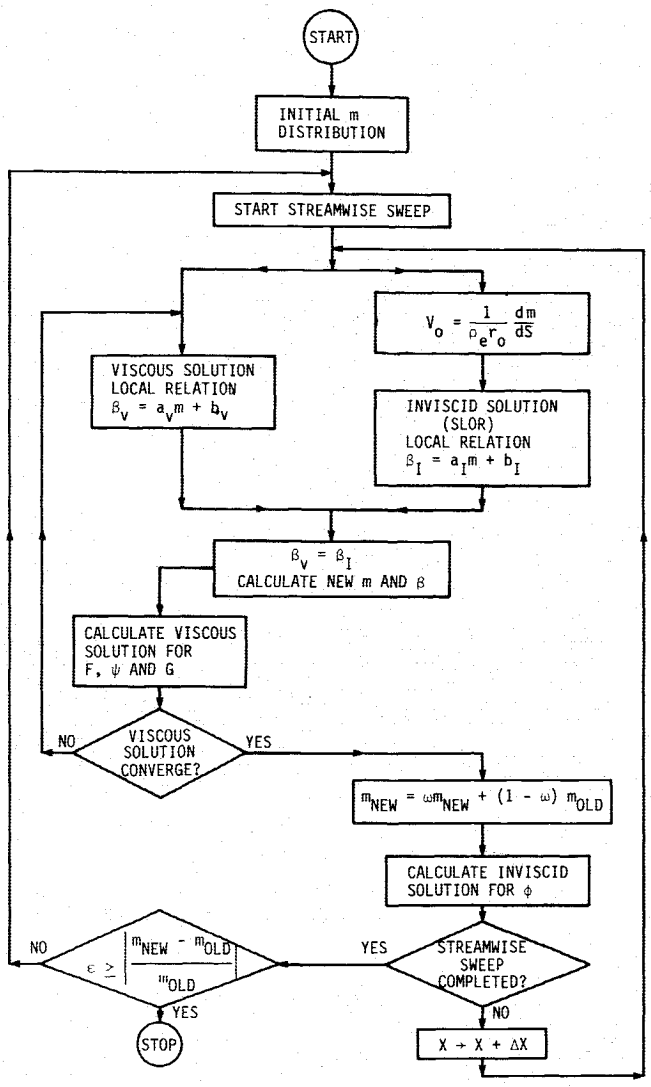

Fig. 1 Flowchart for the simultaneous method.

present study is based on the work of Ref. 15. In this method, the coupling algorithm is given as

$$m^{n+1} = m^n[(1-\omega) + \omega(u_{e,V}/u_{e,I})^b] \tag{16}$$

where $u_{e,V}$ is the edge velocity from the viscous solution, $u_{e,I}$ is the tangential velocity at the surface from the inviscid solution, and b is a constant whose typical value is given as 1.5. Because of the simplicity of the coupling algorithm in the semi-inverse method, an efficient implicit approximate factorization (AF2) scheme introduced by Holst and Ballhaus[18] is used for the inviscid calculation. Empirical values used in the numerical analysis of the full potential equation, mainly the artificial retarded-density coefficient, usually have significant effects on the solution, including the shock strength. Therefore, they are carefully chosen so as to minimize the difference between inviscid solutions of the SLOR and AF2 schemes.

The other distinct difference between the semi-inverse and the simultaneous methods is that in the former, the inviscid solution at each global iteration is required to converge to a certain degree for each updated m distribution. The number of local inviscid iterations between each global interaction is limited to 50. On the other hand, no separate inviscid iteration procedure is used in the simultaneous method. Because of this, the simultaneous method usually requires more global iterations to converge than the semi-inverse method. However, the total computing time of the simultaneous method is considerably smaller than that of the semi-inverse method,

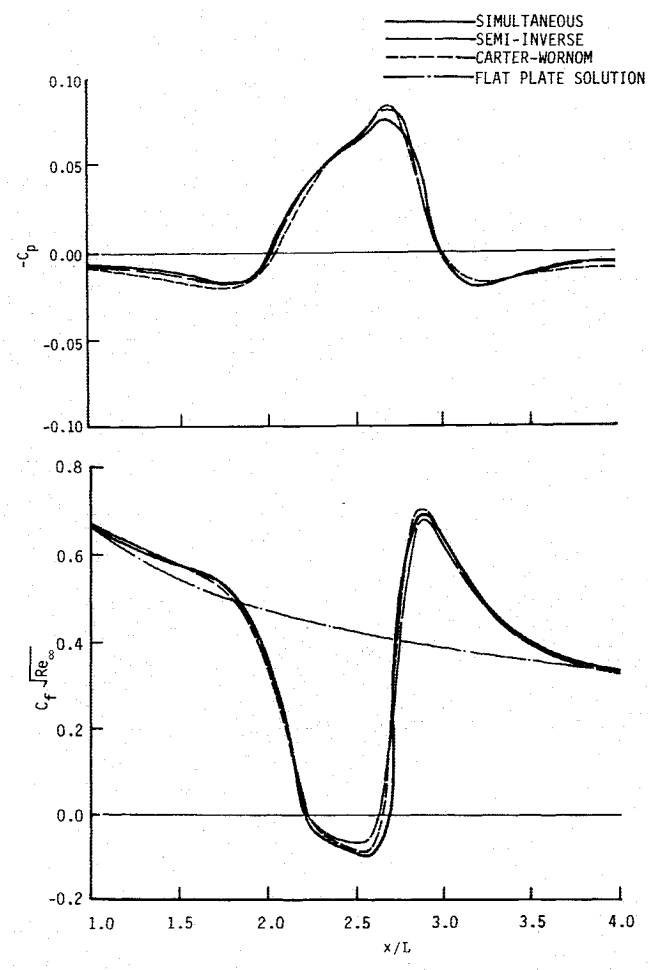

Fig. 2 Incompressible laminar separated flow over a flat plate with a trough.

since each global interaction cycle in the simultaneous method takes only a small fraction of computer time required by the semi-inverse method. Note that the simultaneous method of Edwards and Carter[9] uses a separate inviscid iteration procedure as in the semi-inverse method. This approach is often referred to as a quasisimultaneous interaction method. It should also be noted that $(dm/d\xi)$ terms in Eq. (12) are evaluated by a cubic-spline interpolation method in the semi-inverse method.

The aforementioned interaction methods are used only in the region where viscous-inviscid interaction is presumed to be large and separation may occur. Outside this region, the stable, direct interaction method is applied; i.e., β calculated from the inviscid relation, Eq. (15), is used to evaluate the m distribution in the viscous relation, Eq. (8); and the resulting m is fed back into Eq. (15) in the next global interaction. The initial distribution of m needed to start the present interaction algorithm is provided by solving the boundary-layer equations in the direct mode using pressure data from the inviscid solution obtained with only a few iterations.

III. Results and Discussion

In the following computational examples, the inviscid solutions were obtained with a mesh composed of 101 × 31 grid points that were nonuniformly distributed in the streamwise and normal directions, respectively. Inside the interaction region, the same streamwise grid points were used for both viscous and inviscid solutions, and 65 grid points were allocated. In the normal direction of the viscous mesh, 70 points were placed with variable grid spacing for turbulent flows and

with uniform grid spacing for laminar flows. The convergence criterion of the interaction procedure, ε, was based on the maximum relative change in m during the two consecutive interactions, and the typical value of ε ranged from 1×10^{-3} to 1×10^{-4}.

The performance of the present scheme was first evaluated for a two-dimensional, incompressible, laminar, separated flow over a flat plate with a trough located downstream of the leading edge first studied by Carter and Wornom[20] using an inverse interaction method. This case has often been used to validate the solution schemes for incompressible flows. The surface was prescribed as

$$y = -t \operatorname{sech}(4x - 10) \tag{17}$$

where t, the depth of the trough, was set to 0.03 m. The calculation was performed for the case with $Re = 8 \times 10^4$. For the inviscid flowfield, the inflow and outflow boundaries were set to $x/L = -2.5$ and 7.5, respectively, and the upper boundary was set to $y/L = 5$ (where $L = 1$ m). The interaction region extended from $x/L = 1.0$–4.0. The flow was assumed to be isothermal, and the FLARE approximation was used in the reserved flow regions. The relaxation factor ω was set to 0.5 and 0.7 for the simultaneous and semi-inverse methods, respectively. For the convergence level $\varepsilon = 1 \times 10^{-4}$, the semi-inverse method required 42 iterations; the simultaneous method converged in 90 iterations. However, the simultaneous method required only about half the computing time needed by the semi-inverse method, since each iteration cycle in the simultaneous method took only about 20% of the computing time required by the semi-inverse method. Some results calculated with the present interaction methods are compared with the predictions of Carter and Wornom[20] in Fig. 2. The predictions of the surface pressure and the skin-friction coefficient are in good agreement with those of the inverse method.[20] The reason for the slight disagreement between results of two interaction methods is believed to be that the solution procedures of the inviscid flowfield are different (SLOR and AF2),[18] and the representations of $(dm/d\xi)$ terms in Eq. (12) are different.

The next test case is the transonic flow over an axisymmetric circular-arc bottail with a solid cylindrical plume simulator studied experimentally by Reubush.[21] The detailed description of the boattail configuration is given in Ref. 21. The computations are for the configuration 1 boattail, the steepest boattail tested by Reubush, at the subcritical condition of $M_\infty = 0.7$ and $Re = 1.6 \times 10^7$. The experimental data show extensive separation driven by the strong adverse pressure gradient without the appearance of a shock wave.

The inviscid computational domain extended from $x/d_m = -3.0$–5.5 in the streamwise direction and $y/d_m = 5$ (x is measured from the starting point of boattail, and d_m is the maximum boattail diameter). The interaction region extended from $x/d_m = -1.0$–2.5. The effect of the cone-cylinder forebody was neglected in the present calculations. The transition point from laminar to turbulent flow was assumed to be at $x/d_m = -6.0$. The use of Johnson-King model was initiated at $x/d_m = -1.1$ after starting with the Cebeci-Smith model. In the region of reversed flow, the FLARE approximation was always used. The value of ω was set to 0.35 and 0.50 for the semi-inverse and simultaneous methods, respectively. The convergence behavior of the iteration process depended on the turbulence model used. In the semi-inverse method, the Cebeci-Smith model required about 80 iterations, and the Johnson-King model required 110 iterations for $\varepsilon = 1 \times 10^{-3}$. In the simultaneous method, the turbulence models had little effect on the convergence behavior, and the solutions converged in 185 iterations. In terms of total computing time, the simultaneous method required only about 40% of that needed by the semi-inverse method.

Figure 3 compares the predictions with the experimental data. Only the measurement of the surface pressure is avail-

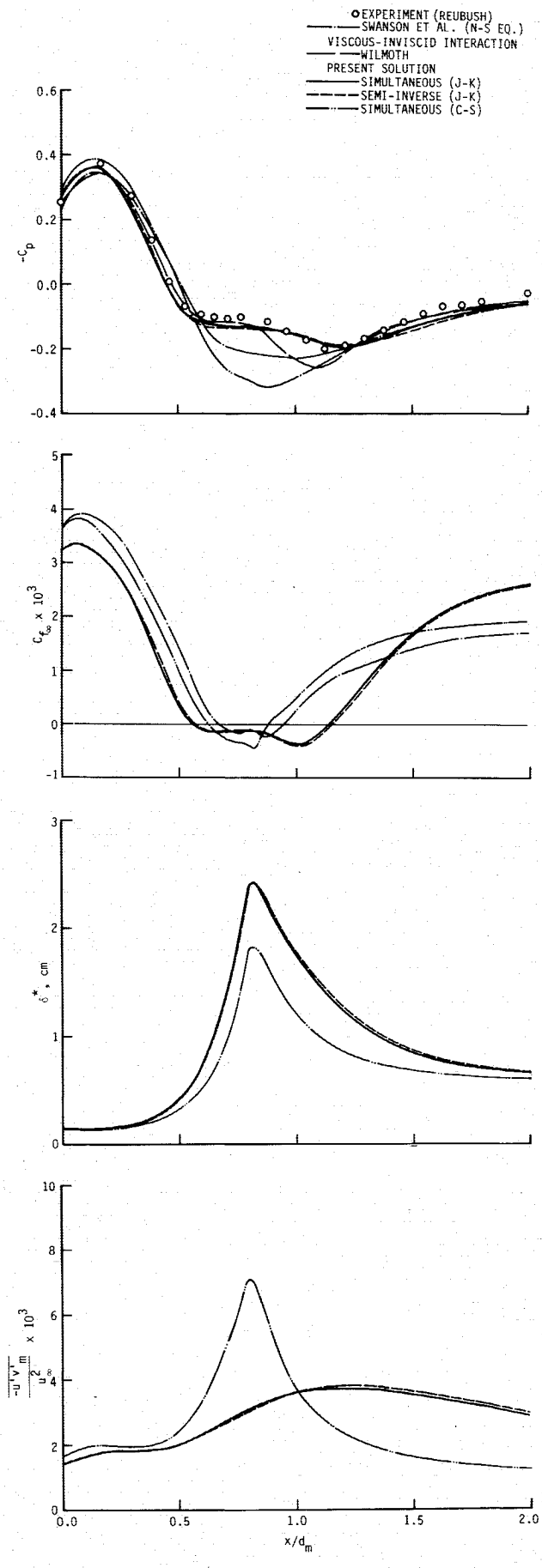

Fig. 3 Transonic turbulent separated flow over a boattail (configuration 1, $M_\infty = 0.7$, $Re = 1.16 \times 10^7$).

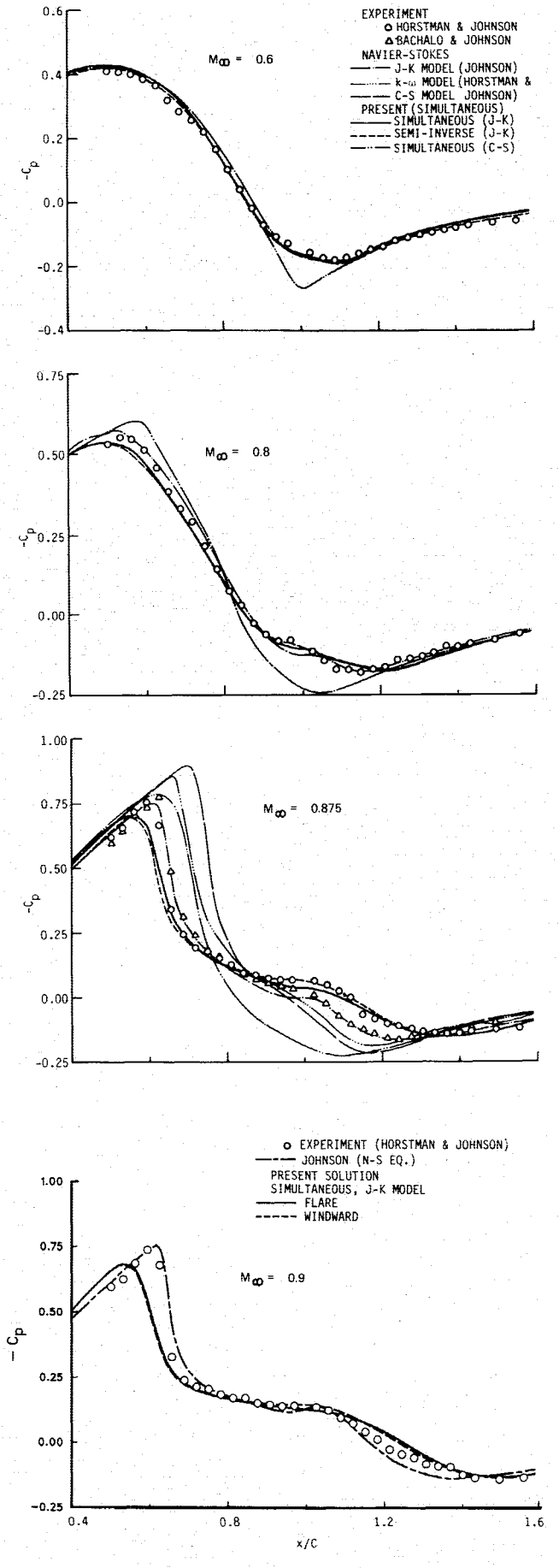

Fig. 4 Comparison of surface pressure distributions for transonic turbulent flow over a bump.

able. Also shown in Fig. 3 are the Navier-Stokes solutions obtained by Swanson et al.[22] using the relaxation-type algebraic-turbulence model of Shang and Hankey[23] and the direct viscous-inviscid interaction results of Wilmoth[24] that used the experimentally determined separation point in the calculation scheme. The present solutions obtained with the Cebeci-Smith model significantly overpredict the surface pressure in the vicinity of the boattail-sting juncture and do not seem to capture the pressure plateau that is characteristic of extensive separation. The separation point determined from the oil flow visualization study[25] was $x/d_m = 0.51$, and the reattachment point is expected to be near $x/d_m = 1.1$. The prediction of these points by the Cebeci-Smith model is also very poor ($x/d_m = 0.64$ and 0.88, respectively). The Navier-Stokes solutions[22] show similar trends. The interaction results by Wilmoth[24] show better agreement with the experimental data than the above results and clearly exhibit the general characteristics of the pressure plateau but show a rapid pressure increase in the second recovery region. On the other hand, the

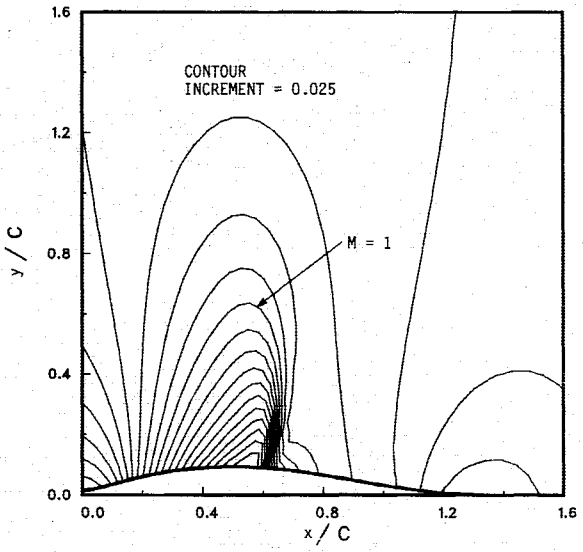

Fig. 5 Mach contour for $M_\infty = 0.875$ flow over a bump.

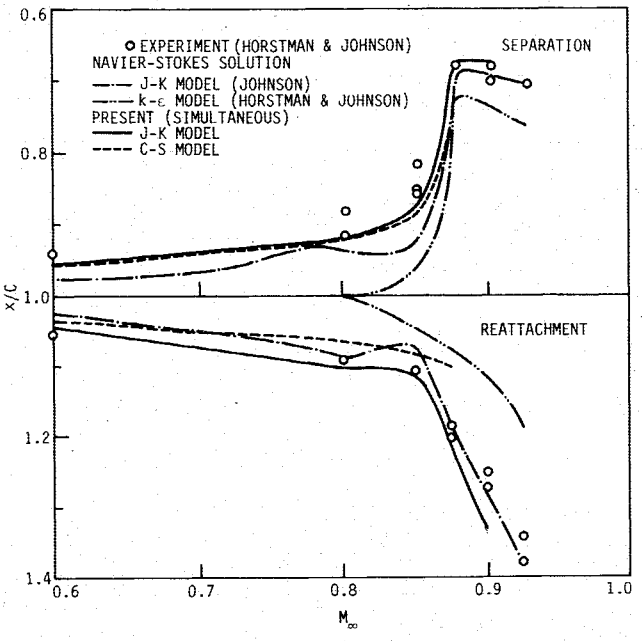

Fig. 6 Comparison of separation and reattachment points for transonic flow over a bump.

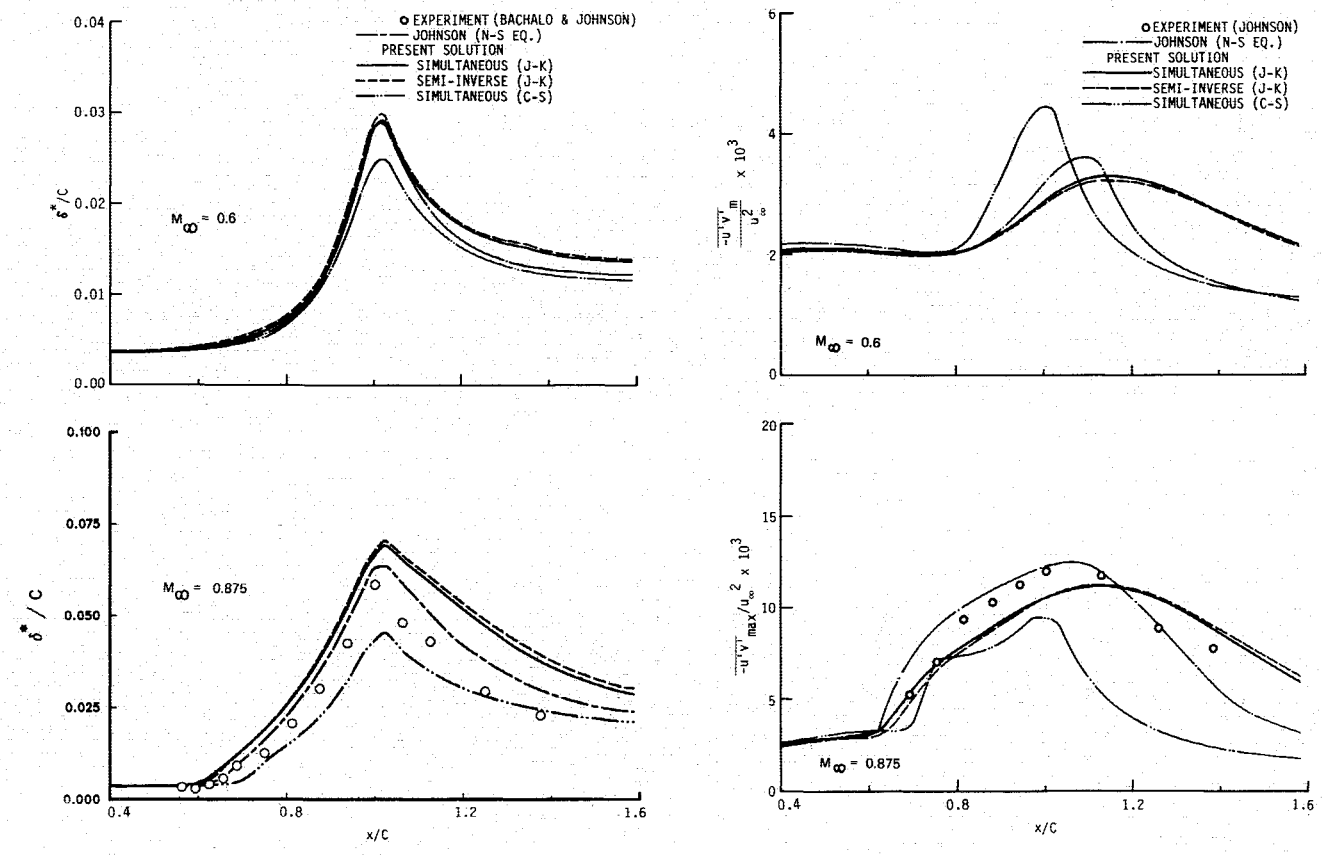

Fig. 7 Comparison of displacement thickness and maximum Reynolds stress distributions for transonic flow over a bump.

present predictions with the Johnson-King model generally agree very well with the experimental data. Particularly, the prediction of the separation and reattachment points ($x/d_m = 0.56$ and 1.15, respectively) is much better. The displacement thickness obtained with the Johnson-King model is larger by as much as 30% than that obtained with the Cebeci-Smith model. The Cebeci-Smith model predicts a sharp peak in $-\overline{u'v'}_m$. On the other hand, $-\overline{u'v'}_m$ predicted with the Johnson-King model shows more gradual increase over a longer streamwise distance, which is responsible for the thick displacement thickness and smaller pressure recovery.

The last example is the shock interacted flowfield about an axisymmetric circular-arc bump attached to a circular cylinder placed parallel to the flow direction studied experimentally by Bachalo and Johnson[26] and Horstman and Johnson.[27] The details of this flow configuration are described in Ref. 26. This model was first tested at $M_\infty = 0.875$ and $Re = 1.36 \times 10^7$ in the NASA Ames 2×2 ft transonic wind tunnel[26] and was later measured over a M_∞ range of 0.4–0.94 in the 6×6 ft supersonic wind tunnel.[27] These experimental data are summarized in Refs. 14 and 27. The inviscid computational domain extended from $x/C = -2.0$–3.0 in the streamwise direction and $2.5C$ in the transverse direction (x is referenced to the forward intersection point of the bump with the cylinder, and C is the length of the bump). The viscous-inviscid interaction region extended from $x/C = -0.5$–1.5. Transition from laminar to turbulent flow was imposed at $x/C = -2.8$. The starting point for the Johnson-King model was $x/C = -0.6$.

The convergence behavior of the interaction procedure was found to be very sensitive to the choice of turbulence model and the freestream Mach number. In subcritical cases, the solutions usually converged well for both interaction methods with a relatively large value of ω regardless of the turbulence models. The semi-inverse method converged in 35–50 iterations with $\omega = 0.7$–1.0 for $\varepsilon = 1 \times 10^{-3}$. The simultaneous method required about 100 iterations with $\omega = 0.7$ for the same ε. For supercritical cases with $M_\infty < 0.9$, the semi-inverse method with the Cebeci-Smith model required about 150 iterations with $\omega = 0.4$–0.6 for $\varepsilon = 1 \times 10^{-3}$. When the Johnson-King model was used in the semi-inverse method, a smaller value of ω (0.2–0.3) was necessary to obtain convergence. However, it has not been possible to reduce ε below 1×10^{-2} due to the oscillatory behavior in the convergence pattern. For $M_\infty = 0.9$, the solution by the semi-inverse method diverged even with a small ω. On the other hand, with the simultaneous method for the supercritical cases with the Mach number up to 0.9, the solutions still converged to $\varepsilon = 1 \times 10^{-3}$ in 200–250 iterations with a relatively large value of ω (0.4–0.7) for both turbulence models. For the supercritical flows, the simultaneous method took only 20–30% of the total computing time required by the semi-inverse method. A typical calculation with the simultaneous method required 60–80 min on a Perkin-Elmer 3240 minicomputer.

Figure 4 compares the calculated surface pressure distributions with the experimental data taken at $M_\infty = 0.6$, 0.8, 0.875, and 0.9. The Navier-Stokes solutions obtained by Johnson[14] using the Johnson-King turbulence model are also compared. For $M_\infty = 0.875$, the Navier-Stokes solutions of Horstman and Johnson[27] based on the Cebeci-Smith and k-ε turbulence models are also displayed. The present solutions with the Cebeci-Smith model overpredict the pressure in the separated region and do not capture the pressure plateau characteristics. The same trend is observed in the Navier-Stokes solutions with the same Cebeci-Smith model. The overall predictions of the present interaction method using the Johnson-King model are observed to agree well in general with the experimental data and the Navier-Stokes solutions[14] obtained with the same turbulence model. However, the shock location was predicted slightly upstream of the measured data, and the disagreement between results of the simultaneous interaction method and the Navier-Stokes solutions became noticeable in supercritical flow cases. The main cause of this disagreement is believed to be attributed to the failure

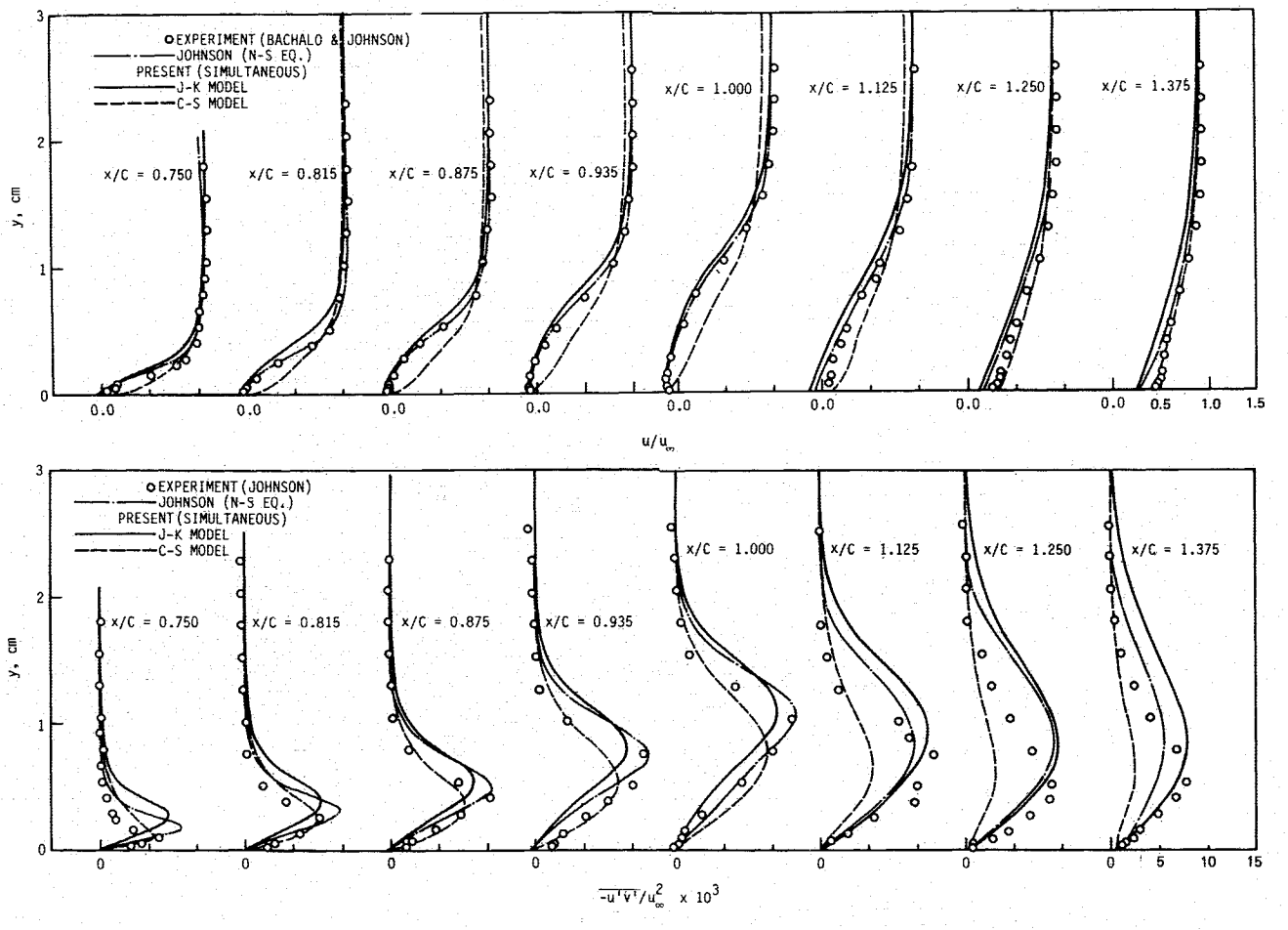

Fig. 8 Comparison of velocity and Reynolds stress profiles for $M_\infty = 0.875$ flow over a bump.

of the boundary-layer approximation because the shock wave penetrates the boundary layer and may generate a significant normal pressure gradient.

The pressure coefficient predicted using the FLARE approximation is compared in Fig. 4 with the predictions using windward differencing for the $M_\infty = 0.9$ case that has the largest separated region among flows considered in the present study. The two solutions gave nearly identical results and exhibited similar convergence behavior. Therefore, it is felt that the use of the FLARE approximation is justified for the flows considered in the present study.

Figure 5 presents a Mach contour plot obtained by the present simultaneous method with the Johnson-King model at $M_\infty = 0.875$. Note that the plot was made using only the inviscid part of the interacted solution. Figure 6 compares the predicted separation and reattachment points with the experimentally observed values and values from the Navier-Stokes solutions.[14,27] The predictions obtained by the simultaneous method with the Johnson-King model are generally in good agreement with the measurements. The reattachment points are predicted slightly downstream of the measured values. The predictions with the Cebeci-Smith model are relatively good for lower M_∞ but become poor as M_∞ is increased above 0.85. On the other hand, the Navier-Stokes solutions[14] with the Johnson-King model are observed to underpredict significantly the separation point compared to the measurements and the present results with the same model. It is also interesting to note that the Navier-Stokes[27] solutions with the k-ε model failed to predict separation when $M_\infty < 0.8$.

The predicted and measured distributions of the displacement thickness and the maximum Reynolds stress are compared for $M_\infty = 0.6$ and 0.875 in Fig. 7. None of the predictions for the displacement thickness agrees well with the measurements over the full extent of the flow. The present solutions with the Johnson-King model predict the largest displacement thickness. In the predictions of $-\overline{u'v'}_m$, the Cebeci-Smith model shows a more rapid increase and abrupt decrease, whereas the Johnson-King model provides more accurate predictions near the shock wave and smoother development across the flowfield. Note that the present predictions with the Johnson-King model indicate a slower decay downstream of the reattachment point than the Navier-Stokes solutions[14] with the same model. The calculated profiles of the mean velocity and Reynolds stress for $M_\infty = 0.875$ are compared with the measurements and Navier-Stokes solutions[14] in Fig. 8. The agreement between predictions with the Johnson-King model and the measurements is especially good in the separated flow region. After the reattachment point, the predictions of the velocity profiles with the Cebeci-Smith model agree better with the measurements. This slow flow recovery downstream of the reattachment point by the Johnson-King model appears to be a shortcoming that requires improvement. The overall predictions of the Reynolds stress with the Johnson-King model show better agreement with the measurements than predictions with the Cebeci-Smith model. However, in the outer region of the boundary layer, the Reynolds stresses predicted with the Johnson-King model decrease too slowly.

IV. Concluding Remarks

The simultaneous interaction method was found to be more efficient and stable over a wider range of flows than the semi-inverse method. It was also found that the accuracy of the solutions is more strongly dependent on the turbulence

modeling than the interaction algorithm. The convergence behavior of the simultaneous method seemed to be relatively insensitive to the turbulence model used. The use of the pseudo-time-dependent approach reduced the total computing time by a factor of 5. The predictions obtained by the FLARE approximation showed good agreement with those obtained by the windward-differencing scheme. The Johnson-King turbulence model was found to provide generally better predictions than the Cebeci-Smith and more sophisticated two-equation models for the transonic separated flows considered.

Acknowledgment

This work was supported by NASA Ames Research Center under Grant NAG-2-152.

References

[1]Lee D. and Pletcher, R. H., "Application of Viscous-Inviscid Interaction Methods to Transonic Turbulent Flows," Iowa State Univ., Ames, IA, TR HTL-42, CFD-16, ISU-ERI-Ames-87055, 1986.

[2]Le Balleur, J. C., "Couplage Visqueux-Non Visqueux: Methode Numerique et Applications Aux Ecoulements Bidimensionnels Transsoniques et Supersoniques," *La Recherche Aerospatiale*, No. 1978-2, March 1978, pp. 65–76.

[3]Carter, J. E., "A New Boundary-Layer Inviscid Iteration Technique for Separated Flow," AIAA Paper 79-1450, July 1979.

[4]Wigton, L. B. and Holt, M., "Viscous-Inviscid Interaction in Transonic Flow," AIAA Paper 81-1003, June 1981.

[5]Wai, J. C. and Yoshihara, H., "Planar Transonic Airfoil Computations with Viscous Interactions," AGARD CP-291, Paper 9, 1981.

[6]Le Balleur, J. C., "A Semi-Implicit and Unsteady Numerical Method of Viscous-Inviscid Interaction for Transonic Separated Flows," *Le Recherche Aerospatiale*, No. 1984-1, 1984, pp. 15–37.

[7]Houwink, R. and Veldman, A. E. P., "Steady and Unsteady Separated Flow Computations for Transonic Airfoils," AIAA Paper 84-1618, June 1984.

[8]Cebeci, T., Clark, R. W., Chang, K. C., Halsey, N. D., and Lee, K., "Airfoils with Separation and the Resulting Wakes," *Proceedings of the 3rd Symposium on Numerical and Physical Aspects of Aerodynamic Flow*, Pt. 2, California State Univ., Long Beach, California, 1985, pp. 13–25.

[9]Edwards, D. E. and Carter, J. E., "A Quasi-Simultaneous Finite-Difference Approach for Strongly Interacting Flow," *Proceedings of the 3rd Symposium on Numerical and Physical Aspects of Aerodynamic Flows*, Pt. 1, California State Univ., Long Beach, California, 1985, pp. 63–73.

[10]Viegas, J. R. and Horstman, C. C., "Comparison of Multiequation Turbulence Models for Several Shock Boundary-Layer Interaction Flows," *AIAA Journal*, Vol. 17, Aug. 1979, pp. 811–820.

[11]Johnson, D. A. and King, L. S., "A Mathematically Simple Turbulence Closure Model for Attached and Separated Turbulent Boundary Layers," *AIAA Journal*, Vol. 23, Nov. 1985, pp. 1684–1692.

[12]Cebeci, T. and Smith, A. M. O., *Analysis of Turbulent Boundary Layers*, Academic Press, New York, 1974,

[13]Kwon, O. K. and Pletcher, R. H., "Prediction of the Incompressible Flow Over a Rearward-Facing Step," Iowa State Univ., Ames, IA, TR HTL-26, CFD-4, ISU-ERI-AMES-82019, 1981.

[14]Johnson, D. A., "Transonic Separated Flow Predictions with an Eddy-Viscosity/Reynolds-Stress Closure Model," *AIAA Journal*, Vol. 25, Feb. 1987, pp. 252–259.

[15]Lee, D. S. and Pletcher, R. H., "Application of a Viscous-Inviscid Interaction Method to Predict Transonic Separated Flows," *Proceedings of the 3rd Symposium on Numerical and Physical Aspects of Aerodynamics Flows,* Pt. 1, California State Univ., Long Beach California, 1985, pp. 75–85.

[16]Reyhner, T. A. and Flügge-Lotz, I., "The Interaction of a Shock Wave with a Laminar Boundary Layer," *International Journal of Nonlinear Mechanics*, Vol. 3, No. 2, June 1968, pp. 173–199.

[17]Lighthill, M. J., " On Displacement Thickness," *Journal of Fluid Mechanics*, Vol. 4, Pt. 4, Aug. 1958, pp. 383–392.

[18]Holst, T. L. and Ballhaus, W. F., "Fast, Conservative Schemes for the Full Potential Equation Applied to Transonic Flows," *AIAA Journal*, Vol. 17, Feb. 1979, pp. 145–152.

[19]Thompson, J. F., Thames, F. C., and Mastin, C. W., "Automatic Numerical Generation of Body-Fitted Curvilinear Coordinate System for Field Containing Any Number of Arbitrary Two-Dimensional Bodies," *Journal of Computational Physics*, Vol. 15, No. 3, July 1974, pp. 299–319.

[20]Carter, J. E. and Wornom, S. F., "Solutions for Incompressible Separated Boundary Layers Including Viscous-Inviscid Interaction," NASA SP-347, 1975.

[21]Reubush, D. E., "Experimental Study of the Effectiveness of Cylindrical Plume Simulators for Predicting Jet-On Boattail Drag at Mach Numbers up to 1.30," NASA TN D-7795, 1974.

[22]Swanson, R. C., Rubin, S. G., and Khosla, P. K., "Calculation of Afterbody Flows with Composite Velocity Formulation," AIAA Paper 83-1736, July 1983.

[23]Shang, J. S. and Hankey, W. L., Jr., "Numerical Solution for Supersonic Turbulent Flow over a Compression Ramp," *AIAA Journal*, Vol. 13, Oct. 1975, pp. 1368–1374.

[24]Wilmoth, R. G., "Computation of Transonic Boattail Flow with Separation," NASA TP-1070, 1977.

[25]Abeyounis, W. K., "Boundary-Layer Separation on Isolated Boattail Nozzles," NASA CR-152703, 1977.

[26]Bachalo, W. D. and Johnson, D. A., "An Investigation of Transonic Turbulent Boundary-Layer Separation Generated on an Axisymmetric Flow Model," AIAA Paper 79-1479, July 1979.

[27]Horstman, C. C. and Johnson, D. A., "Prediction of Transonic Flows," *AIAA Journal*, Vol. 22, July 1984, pp. 1001–1003.